

Arduino Uno-based colorimetric sensor Traction Control System 3200 with AgNPs/PVP for Hg²⁺ detection in river water of Aceh Selatan Regency, Indonesia

Khairi Suhud^{1*} , Rizka Amalia¹, Muhammad Syukri Surbakti², Rinaldi Idroes³ , Lelifjari¹, Sagir Alva⁴ , Halimahtussadiyah Ritonga⁵, Mazwan⁶, Muhammad Daffa Hadistya¹, Andriy Anta Kacaribu⁷ 

¹ Department of Chemistry, Faculty of Mathematics and Natural Sciences, Universitas Syiah Kuala (USK), Banda Aceh 23111, Indonesia

² Department of Physics, Faculty of Mathematics and Natural Sciences, Universitas Syiah Kuala (USK), Banda Aceh 23111, Indonesia

³ Department of Pharmacy, Faculty of Mathematics and Natural Sciences, Universitas Syiah Kuala (USK), Banda Aceh 23111, Indonesia

⁴ Department of Mechanical Engineering, Faculty of Engineering, Mercu Buana University, Jakarta 11650, Indonesia

⁵ Department of Chemistry, Faculty of Mathematics and Natural Sciences, Universitas Halu Oleo, Kendari 93232, Indonesia

⁶ Department of Geography Education, Universitas Al-Washliyah, Banda Aceh, 23111, Indonesia

⁷ Doctoral Program of Agricultural Sciences, Postgraduate School, Universitas Syiah Kuala (USK), Banda Aceh 23111, Indonesia

* Corresponding author's e-mail: khairi@usk.ac.id

ABSTRACT

This study developed a colorimetric sensor using an Arduino Uno-based Traction Control System 3200 (TCS3200) color sensor and silver nanoparticles stabilized by polyvinyl-pyrrolidone (AgNPs/PVP) for detecting Hg(II) ions in river water samples from Aceh Selatan Regency. AgNPs/PVP exhibited localized surface plasmon resonance (LSPR) at 400 nm, with particles sized between 5.4 and 15.5 nm. Upon exposure to Hg²⁺, a visible color change indicated detection capability, with recovery rates of 97.3–100% and detection limits at 1.8 and 6 µg/L, respectively. Colorimetric results matched UV-Vis spectrophotometry, validating reliability. This efficient method provides a viable option for Hg²⁺ monitoring in environmental samples.

Keywords: Arduino Uno, pollutant detection, integrated development environmental software, ion mercury, TCS3200 color sensor.

INTRODUCTION

Mercury, despite its severe impact on health, continues to be mined for various purposes, including gold mining, electronic applications, and chemical manufacturing (Ahmad et al., 2022; Nisah, et al., 2022). Inevitably, mercury pollution poses a significant threat to human health due to its acute toxicity and genotoxicity (Sánchez-Alarcón et al., 2021). This necessitates the development of analytical methods that are not only sensitive and accurate but also cost-effective and easy to

operate for Hg²⁺ detection (Balasurya et al., 2020; Schiesaro et al., 2020). Previous studies have demonstrated that mercury can be detected using silver nanoparticles (AgNPs) as an indicator (Monisha et al., 2021). However, the stability of AgNPs as an indicator for Hg²⁺ detection remains low. To address this limitation, polyvinylpyrrolidone (PVP) has been utilized to stabilize AgNPs, acting as both an immobilizing and anti-agglomeration agent (Chen et al., 2019; Zhou et al., 2014).

Traditional methods for detecting mercury in environmental waters, such as atomic absorption

spectrometry (AAS), inductively coupled plasma-atomic emission spectrometry (ICP-AES), high-performance liquid chromatography (HPLC), and UV-Vis spectrophotometry, have been widely used (Hasan et al., 2020; Huang et al., 2021). While UV-Vis spectrophotometry offers simplicity and satisfactory accuracy for colored compounds, it struggles with colorless Hg^{2+} -contaminated samples and has drawbacks, including lack of portability, complex operation protocols, high costs, and requires trained operators (Janani et al., 2020). This study addresses these limitations by developing a portable, low cost, and simple analytical method using a TCS3200-based colorimetric sensor, which enhances detection efficiency for Hg^{2+} in real-world river samples.

The sensor system developed in this work is a colorimetric sensor Traction Control System 3200 (TCS3200). Colorimetric sensor TCS3200 is a light sensor programmed to translate red, green, and blue (RGB) colors into frequencies comprised of the configuration of 8×8 photodiodes (Fernández-Ramos et al., 2020; Singh et al., 2020). Colorimetric sensor TCS3200 has been widely reported for its analytical applications viz. determining concentrations of cyanide (Singh et al., 2020), nitrogen (Sandra et al., 2020), heavy metals (Fitri et al., 2019), borax (Suhud et al., 2024), and rhodamine B (Surbakti et al., 2022). In the case of colorimetric sensor, analytes should be firstly reacted with complexing agent to induce the color changing (Amirjani and Fatmehsari, 2018; Monisha et al., 2021). In this present study, the sensor detects color degradation from the cuvette filled with an indicator, thereby increasing the sensitivity specifically to analyze mercury ions (Hg^{2+}) pollutions. Indicator used in this regard was AgNPs/PVP which could induce the color transformation from yellow to colorless when reacted with mercury ion solutions (Amirjani and Fatmehsari, 2018).

The color intensity corresponds to the mercury concentration which is converted through sensor pin output as a square signal. The signal with varied frequencies is then processed using micro-controller in Arduino Uno. This color processing uses four filters, namely red, green, blue, and ‘no filter’. In this present study, ‘no filter’ was not included because the three parameters are considered adequate to represent the color degradation of mercury in the sample (Brambilla et al., 2021). Filter settings were performed by administering ‘low’ and ‘high’ logics into the Arduino IDE program (Surbakti et al., 2022). The distance between sample

and 8×8 diode array was kept 3 cm, following the sensor system geometry. Console color was made dark so that the noise from external light could be reduced. After the concentration of mercury obtained using the Arduino Uno-based colorimetric sensor TCS3200, the results were then compared with the standardized UV-Vis spectrophotometer methods, as suggested by a previous report (Hasan et al., 2020; Huang et al., 2021).

MATERIALS AND METHODS

Materials and equipment

Chemicals used were HgCl_2 , AgNO_3 , polyvinyl pyrrolidone (PVP), HNO_3 , HCl , NaOH , $\text{Cr}(\text{NO}_3)_3 \cdot 9\text{H}_2\text{O}$, CaCl_2 , $\text{FeCl}_2 \cdot 4\text{H}_2\text{O}$, NaCl , $\text{NiSO}_4 \cdot 6\text{H}_2\text{O}$, $\text{Pb}(\text{NO}_3)_2$, $\text{Co}(\text{NO}_3)_2 \cdot 6\text{H}_2\text{O}$, $\text{CuSO}_4 \cdot 5\text{H}_2\text{O}$, ZnCl_2 , and borohydride, where all of which were purchased from Merck (Selangor, Malaysia) in pro-analytical grade. The mercury-contaminated samples were collected from the River in Aceh Selatan Regency, Aceh Province, Indonesia.

Instruments and equipment used for this study were UV-Vis spectrophotometer (Thermo Fisher Scientific, Selangor Malaysia), a colorimetric sensor TCS3200 (ICTAOS/AMS), an Arduino Uno console (Wavgat), Transmission Electron Microscope (TEM) (TEM HT7700, Hitachi Ltd Japan), and Fourier Transform Infrared (FTIR) Spectroscopy (FT-IR IRPrestige-21, Shimadzu Japan).

Preparation and characterization of AgNPs/PVP

The preparation of AgNPs/PVP followed a method reported previously (Monisha et al., 2021). PVP 1% made by dissolving 1 g PVP into 100 mL aquades (1 mL), AgNO_3 0.1 M (0.1 mL), and distilled water (20 mL) were inserted into a 50-mL volumetric flask, stored in an ice bath with a constant stirring (1000 rpm; 30 min). Thereafter, 1 mL NaBH_4 0.02 M was drop-wised into the mixture and stirred until the colorless solution turned into bright yellow indicating the formation of AgNPs/PVP. To determine the morphological shape and its functional groups, the characterizations were performed employing TEM and FT-IR, respectively.

Hardware design

Firstly, the console for colorimetric sensor TCS3200 was assembled before connected to the output port of the sensor through a jumper cable

into the Arduino Uno microcomputer for the frequency data processing and conversion into 8-bit RGB digital data. There were 256 variations of color digits for every RGB color component which could be sorted and differentiated through the processing. Variation of color digits was displayed on a computer screen and modified to reduce the color variation. The color variation was recorded in.xls (Microsoft Excel). The hardware setting has been presented in n Figure 1.

Development of the TCS3200 sensor console

Console for the sensor TCS3200 was designed in a black color to absorb all color wavelengths. The distance between diode array and the color object was 3 cm. The console was arranged so that the light from the outside could not enter. The sensor TCS3200 was positioned against the color sample which would be absorbed into the

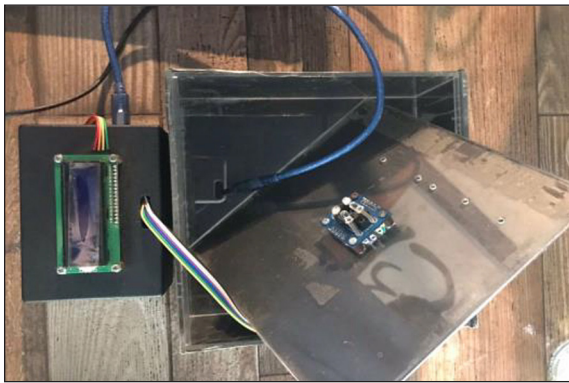


Figure 1. The hardware design

cuvette. Four LED units with a white wavelength would pass through the solution in the cuvette, and the diode array acted by reflecting the light intensity following the intensity of sample color.

Software design

Blink test was performed on the Arduino Uno system to detect the response and the performance of the microcomputer. The software used was Arduino IDE with an open-source library for programming C language. The program library was modified to activate the necessary color filter, Arduino Uno pin, required display format, and data storage mode. The display of the software used (Arduino IDE) presented in Figure 2.

Mercury ions (Hg^{2+}) analysis using the colorimetric sensor TCS3200

Calibration curve construction and validation

Standard solution of Hg^{2+} with varied concentrations (10, 20, 30, 40, 50, 60, and 70 $\mu\text{g/L}$) were prepared from a stock mercury solution (1 mg/L). Each solution was pipetted 1 mL and added into a vial containing 2 mL AgNPs/PVP solution. The mixture was left for 5 min before the determination at maximum wavelength using the colorimetric sensor TCS3200. Using the determined maximum wavelength, the signal was generated for each mercury concentration, performed in triplicate and averaged. Thereafter, the RGB values were converted into color index Hue, Intensity,

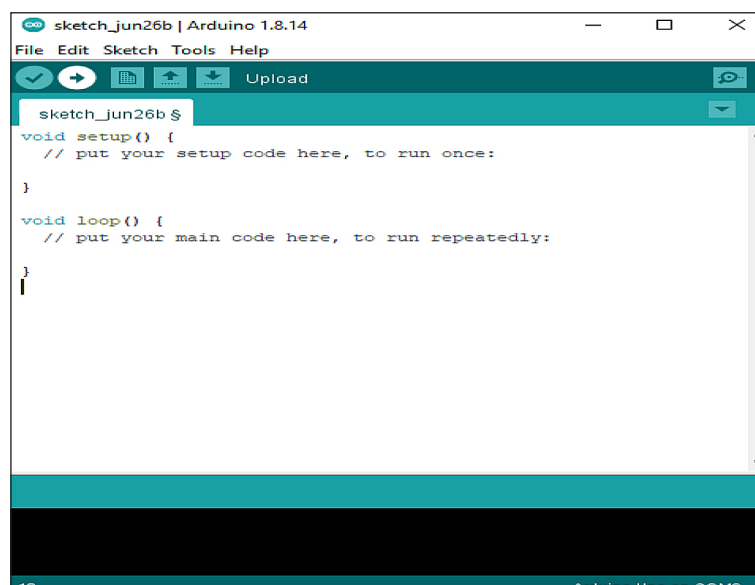


Figure 2. Display of the Arduino IDE Software main menu (Surbakti et al., 2022)

and Saturation (HIS) by using Equation 1, 2, and 3, respectively, as expressed below:

$$I_R = \frac{R}{R+G+B} \quad (1)$$

$$I_G = \frac{G}{R+G+B} \quad (2)$$

$$I_B = \frac{B}{R+G+B} \quad (3)$$

where: I_R, I_G, I_B , are color index of red, green, and blue, respectively.

Model for the HIS color was designed resembling the human visual perception, while the RGB resembling the image of the system display (Brambilla et al., 2021). HIS values were plotted as dependent variables (y-axis) against the concentration variation (x-axis). The method and its calibration curve were subjected for analytical validation based on the accuracy, precision, sensitivity, linearity, selectivity, and specificity, where the calculation for each parameter has been previously described in details (Shukla et al., 2019).

Collected and preparation of the river water samples

The river water samples were collected using purposive sampling technique from five locations along the river, ranging from downstream to upstream, identified as sites A, B, C, D, and E. The geographical coordinates for these locations are presented in Table 1. Sampling was conducted in March 2022, during the dry season. The site was carefully approached to avoid stirring up sediment, water was collected at a mid-stream location while avoiding stagnant areas at a depth of approximately 30–35 cm below the river surface, the container was filled slowly to prevent air bubbles with minimal headspace left to avoid oxidation, each container was labeled with the site ID, date, and time of collection, and the samples were placed in a cooler box with ice packs to maintain temperature stability during transport to the laboratory.

The river water samples were preserved by adding HNO_3 and being stored at low temperatures (4°C). The destruction process was performed to convert the metal contents into their free form. Initially, the sample was filtered using vacuum filter and filter paper, then 20 mL of the sample was taken and mixed with 5 mL NaOH_2 M in a Beaker glass and left for 10 min. Afterward, the mixture was filtered through a filter paper and added with 5 mL HCl_2 M before precipitated and stored for 15 min whilst the pH was sustained at its initial level. The water sample was prepared by means of ‘standard addition’, where the analyte with unknown concentrations were added with a fixed standard solution. This was performed to minimize the errors during the sample preparation and analysis, as suggested previously (Pomal et al., 2021). The sample was determined for its mercury content based on the newly developed colorimetric sensor TCS3200 and reference method – UV-Vis spectrophotometry as a comparative-methods.

Quantification of the Hg^{2+} content

The prepared sample was added together with AgNO_3/PVP into a beaker glass before inserted into a cuvette. The mercury content was determined using the colorimetric sensor TCS3200, where the concentration was derived from the linear equation obtained from the priorly constructed calibration curve. The protocol for this measurement followed the guidelines published previously (Ren et al., 2021).

Statistical analysis

The $\text{Hg}(\text{II})$ concentration results obtained from the TCS3200 + AgNPs/PVP sensor were statistically compared with those from UV-Vis spectrophotometry using a two-sample t-test, as suggested by previous studies (Wang et al., 2024; Wang et al.,

Table 1. Coordinate of locations of the river water sample collection

Samples	Altitude above sea level (m)	Coordinate locations		Initial pH
		N	E	
A	34	3.154594°	97.374343°	7.6 ± 0.1
B	33	3.154467°	97.37438°	7.6 ± 0.1
C	32	3.1543816°	97.373614°	7.6 ± 0.1
D	32	3.154566°	97.374376°	7.6 ± 0.1
E	31	3.154876°	97.376645°	7.6 ± 0.1

Note: N - north; E - east.

2024). A deviation was considered significant if the experimental exceeded the theoretical value. This comparative analysis reinforces the method's precision by aligning sensor readings with established spectrophotometric results.

RESULTS AND DISCUSSION

Maximum wavelength for mercury determination

The UV-Vis spectra of AgNO_3/PVP and a mixture of AgNO_3/PVP and Hg^{2+} 30 $\mu\text{g/L}$, obtained from the measurement at a range of 300–475 nm (Tanvir et al., 2019), presented in Figure 3. A clear spectral peak was observed at 400 nm (absorbance: 0.885 a.u.) assigned as the maximum wavelength. Similar peak still occurred after the addition of Hg^{2+} 30 $\mu\text{g/L}$ at the same wavelength but with reduced absorbance intensity (0.629 a.u.). The spectral peak is indicative to the formation of AgNPs, where the absorbance intensity corresponds to the amount of AgNPs formed (Lin et al., 2016; Xu et al., 2016). This finding is associated to the local surface plasmon resonance (LSPR), which was induced by the light emission at certain wavelengths into the nanoparticle surface resulting to the oscillation of electrons. This is in line with a previous report that found the LSPR of AgNPs at around the same wavelength (Abdel-Lateef et al., 2022; Kemala et al., 2022; Q. Zhou et al., 2016; Zhu et al., 2021).

Characteristics of AgNPs/PVP

FT-IR

Functional group characterization was carried out using FT-IR on the AgNO_3/PVP and after the addition of Hg^{2+} (0.5 mg/L), as shown in Figure 4. From the spectral profile, AgNO_3/PVP was revealed to possess C=O and C-N moieties of the PVP interacting in coordinate covalent bond with the AgNPs (Meenakshi et al., 2019). When mixed with Hg^{2+} (0.5 mg/L), it was observed to cause the broadening of absorbance band at 3319 cm^{-1} and shifted to 3322–3319 cm^{-1} . The spectral peak at 1635 cm^{-1} was assigned to the stretching vibration of C=O and shifted to 1637 cm^{-1} . Shifted wavenumber and change in the transmittance intensity were associated with the interaction between the mercury ions with O-H and C=O moieties in AgNO_3/PVP (Rahmi et al., 2022; Rajar et al., 2021). As for the peaks emerged at 1225 and 1172 cm^{-1} were assigned to the stretching vibrations of C-N and C-O, respectively. Meanwhile, the strong stretching vibrations of C-N and C-O could be observed at the range of 638–457 cm^{-1} . This suggests the presence of the bonding between mercury and the moieties of interest, where the same phenomena were observed at 600–400 cm^{-1} in a previous report (Tanvir et al., 2019).

TEM

Before and after the addition of Hg^{2+} 0.5 mg/L, AgNPs/PVP samples were characterized using TEM to identify the particle shape and size, as

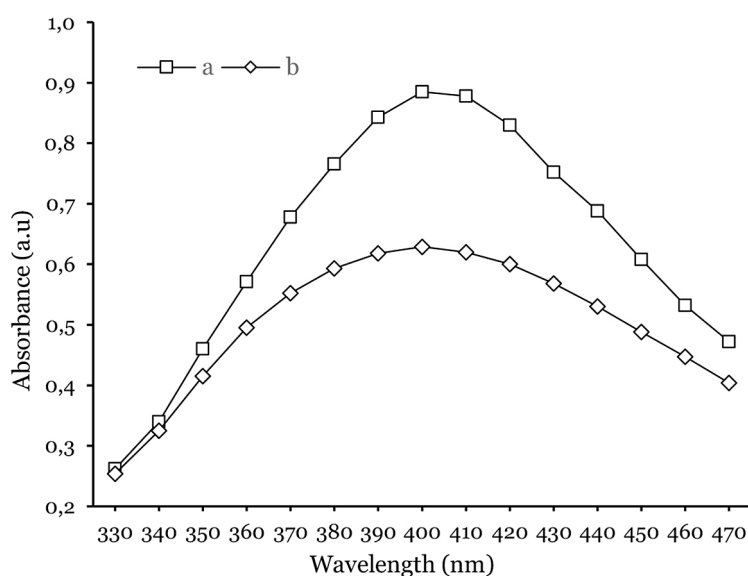


Figure 3. UV-Vis spectra of AgNO_3/PVP (a) and $\text{AgNO}_3/\text{PVP} + \text{Hg}^{2+}$ 30 $\mu\text{g/L}$ (b). The maximum wavelength was found at 400 nm

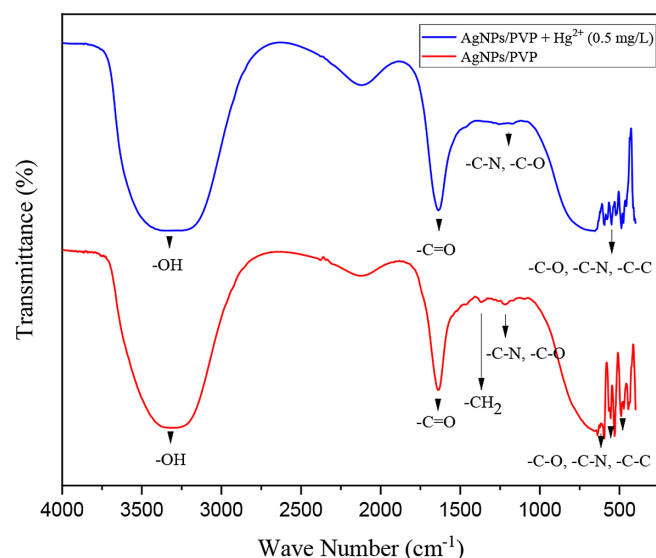


Figure 4. FT-IR spectra of AgNPs/PVP (Red) and AgNPs/PVP + Hg²⁺ (0.5 mg/L, blue)

presented in Figure 5. The particles have a spherical shape with the average diameter sizes ranged from 5.4–15.5 and 2.0–6.5 nm for AgNPs/PVP as a neat solution and as a mixture with Hg²⁺ 0.5 mg/L, respectively. The particle sizes fall into the nano-size category, suggesting the success of NPs formation by the NaBH₄ as the reductant. The nano-size particles further stabilized by the PVP that inhibited the particle size growth and agglomeration (Diamai and Negi, 2020). Reduced particle size following the addition of Hg²⁺ was stipulated due to the formation of mercury NPs since it has higher reduction potential (+0.85 V) than that of Ag⁺ (+0.80 V) (Shrivastava et al., 2019).

Calibration curves based on RGB indices

The calibration curves for the measurement of aqueous mercury based on RGB indices, where each yielded its own regression linear

equation, have been presented (Fig. 6). On the basis of the R² value, I_B generated the most linear curve (R² = 0.9894) with a linear equation of $y = 0.0005x + 0.1144$. This is line with a previous that selected the calibration curve based on the R² value (Nisah et al., 2022). Therefore, I_B-based calibration curve would be further used to determine Hg²⁺.

Determination of Hg²⁺ in the river water sample using UV-Vis spectrophotometer

The calibration curve was constructed based on the AgNPs/PVP + Hg²⁺ mixture with Hg²⁺ concentration ranged from 10 to 70 µg/L at 400 nm, as presented in Figure 7. The linear regression equation obtained was $y = -0.0007x + 0.6486$ with R² = 0.9982. This suggests that the absorbance was dependent to the Hg²⁺ concentrations and inversely correlated with the Lambert-Beer law (Galatage et al., 2021).

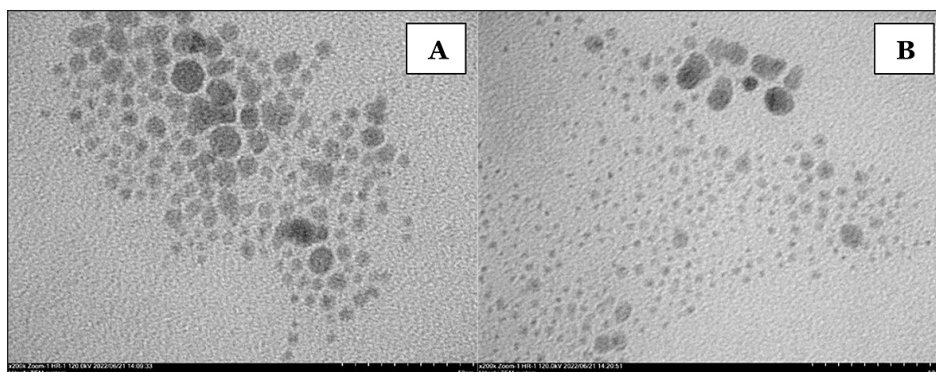


Figure 5. TEM images of AgNPs/PVP (a) and a mixture of AgNPs/PVP and Hg²⁺ 0.5 mg/L (b), observed under 200× magnification

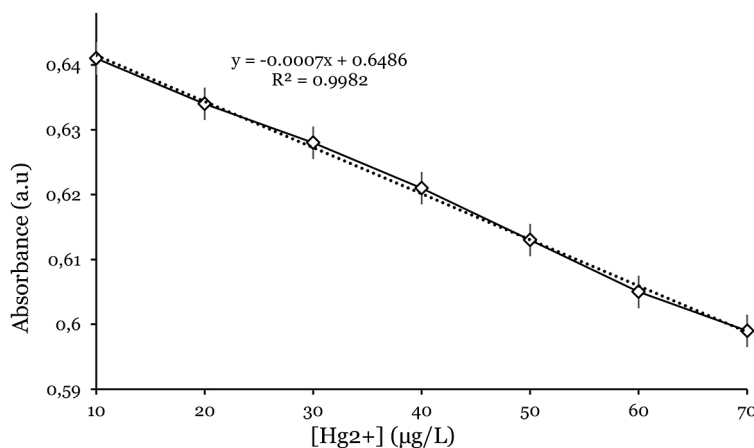


Figure 6. Calibration curves constructed based on I_R (red), I_G (green), and I_B (blue) for aqueous Hg^{2+} determination ($n = 3$)

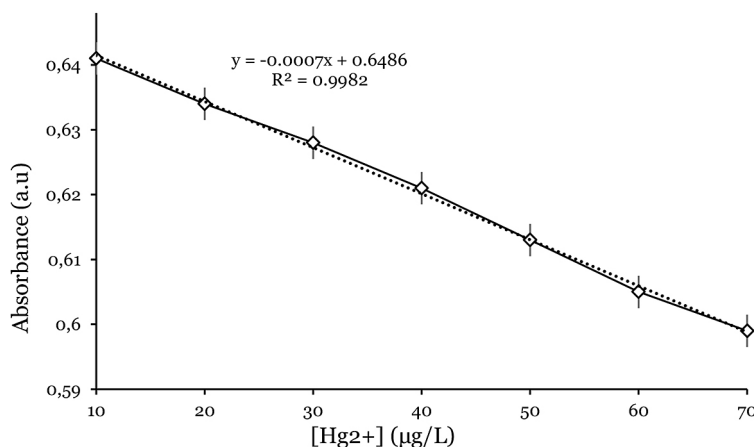


Figure 7. Calibration curve for Hg^{2+} measurement using UV-Vis spectrophotometer

Method validation analysis

Accuracy

Accuracies of the analytical methods was judged based on the recovery (%) that was calculated at concentrations of 10, 30, 50, and 70 $\mu\text{g/L}$ with results presented in Table 2. For the proposed colorimetric method, the recovery was obtained in the range of 97.3–100%. Meanwhile, for the UV-Vis spectrophotometry method, the

recovery ranged from 98.9–108.5%. As per the consensus from an already published report, the acceptable range of recovery should be within 80–120% (Gusrizal et al., 2019). Hence, the accuracies of both methods used in this study are acceptable.

Precision

The precision was measured based on the intra- and inter-day deviation of the data, expressed

Table 2. Recovery percentages of the colorimetric sensor and UV-Vis spectrophotometer

[Hg^{2+}] ($\mu\text{g/L}$)	Calculated conc. ($\mu\text{g/L}$)		Recovery (%)	
	TCS3200	UV-Vis	TCS3200	UV-Vis
10	10.0 ± 0.20	10.8 ± 0.20	100.0 ± 0.01	108.5 ± 0.01
30	29.2 ± 0.06	29.4 ± 0.05	97.3 ± 0.01	98.9 ± 0.01
50	49.2 ± 0.06	50.8 ± 0.06	98.4 ± 0.01	101.7 ± 0.02
70	69.2 ± 0.09	70.8 ± 0.06	98.8 ± 0.02	101.2 ± 0.01

Note: Conc – concentration.

as variation coefficient (VC, %) (Table 3). Using the initial analyte concentrations of 10, 30, 50, and 70 µg/L, we observed a little change in both intra- and inter-day measurements. The VCs, however, were higher in the measurements using the colorimetric sensor than that of UV-Vis spectrophotometer when both were performed on the same day (0.684–0.840% versus 0.156–0.167%) and on different days (0.671–0.869% versus 0.156–0.168%). All values of the VC obtained herein were below 2% (Table 3). Accordingly, the analytical methods used for the determination of Hg²⁺ concentration were considered to have good precision (Amata-tongchai et al., 2019). These findings were supported by the visual observation of the samples, where the color change was not apparent.

Linearity and sensitivity

Based on the constructed calibration curves, the linearities (a parameter to judge the sensor's response) (Nisah, et al., 2022) of both used analytical methods were good as their R² values approaching one ($y = 0.0005x + 0.1144$ and $-0.0007x + 0.6486$ for TCS3200 color sensor and UV-Vis spectrophotometer, respectively) as shown in Figure's 6 dan 7. As for the sensitivity, the quality was judged by the slope of the linear regression equation obtained from the calibration curve. Colorimetric sensor TCS3200 had the slope of 0.0005, while the UV-vis spectrophotometer – 0.0007. Thereafter, the LOD and LOQ for each method

were calculated. The LODs of the colorimetric sensor TCS3200 and UV-vis spectrophotometer were 1.80 and 1.71 µg/L, respectively. Meanwhile, the LOQs for the Hg²⁺ measurements based on colorimetric sensor TCS3200 and UV-vis spectrophotometer were 6.00 and 5.71 µg/L, respectively. The LOD of the TCS3200 colorimetric sensor for Hg(II) was determined to be 1.80 µg/L, which is below the maximum contaminant level goal (MCLG) for mercury of 2 µg/L as established by the U.S. Environmental Protection Agency (EPA) for mercury in drinking water (Environmental Protection Agency, 2024). This finding indicates that the sensor has sufficient sensitivity to detect mercury at concentrations that align with health-protective regulatory thresholds. Therefore, the developed method demonstrates practical applicability for environmental monitoring, particularly for initial screening of water bodies where mercury contamination poses a significant public health concern. By meeting the EPA's stringent criteria, this portable and cost-effective approach could serve as a valuable tool in regions with limited access to advanced laboratory infrastructure.

Selectivity

When AgNO₃/PVP was added with NaCl, NiSO₄, Co(NO₃)₂, Pb(NO₃)₂, FeCl₂, CuSO₄·5H₂O, and Cr(NO₃)₃, 10 mg/L respectively, the color remained bright yellow without changing to colorless (Fig. 8). On contrary, the addition of HgCl₂

Table 3. VC values for colorimetric sensor TCS3200 and UV-Vis spectrophotometer obtained from the intra- and inter-day repetitions

Hg ²⁺ (µg/L)	Intra-day variation coefficient (%)		Inter-day variation coefficient (%)	
	TCS3200	UV-Vis	TCS3200	UV-Vis
10	0.840 ± 0.001	0.156 ± 0.001	0.869 ± 0.001	0.156 ± 0.001
30	0.763 ± 0.001	0.159 ± 0.001	0.787 ± 0.001	0.159 ± 0.001
50	0.714 ± 0.001	0.163 ± 0.001	0.709 ± 0.001	0.164 ± 0.001
70	0.684 ± 0.001	0.167 ± 0.001	0.671 ± 0.001	0.168 ± 0.001



Figure 8. Visual appearance of the AgNPs/PVP solution colors with the addition of NaCl, FeCl₂, NiSO₄, Cr(NO₃)₃, HgCl₂, CuSO₄·5H₂O, Co(NO₃)₂, and Pb(NO₃)₂, respectively

resulted the color change into colorless (Fig. 8), indicating the selectivity of AgNO_3/PVP toward Hg^{2+} . This further corroborated by the measurement of each mixture using colorimetric sensor TCS3200 and UV-vis spectrophotometer, as presented in Figure 9 and 10, respectively. The selectivity of AgNO_3/PVP toward Hg^{2+} was proven by the low I_B value which corresponds to the disappearance of specific yellow color after the addition of Hg^{2+} . When the analyte (Hg^{2+}) is increased in concentration, the I_B score is expected to increase as the absorbance falls concomitant to the oxidation of Ag^0 to Ag^+ by Hg^{2+} (Puchum et al., 2019).

Analysis of aqueous Hg^{2+} using AgNP/PVP on colorimetric sensor TCS3200

The AgNPs/PVP sensor detects $\text{Hg}(\text{II})$ ions through a redox reaction that results in visible

color change. When $\text{Hg}(\text{II})$ ions interact with AgNPs, electron transfer causes the AgNPs to oxidize, leading to color fading. This specific interaction is enhanced by PVP, which stabilizes AgNPs and prevents premature agglomeration, making the sensor highly selective for $\text{Hg}(\text{II})$ ions. The aqueous Hg^{2+} analysis was performed qualitatively by observing the color change after the addition of river water sample (suspected to contain Hg^{2+}) into AgNPs/PVP solution. The occurrence of color changing (owing to the spontaneous oxidation of Ag^0) indicates the presence of Hg^{2+} contamination in the river water (Fiorati et al., 2020; Jabbar et al., 2023; Sakly et al., 2017). For quantitative analysis, the RGB and HIS values were collected through colorimetric sensor TCS3200, as presented in Table 4. Thereafter, the concentration of Hg^{2+} was calculated by substituting y in the priorly obtained linear regression equation with

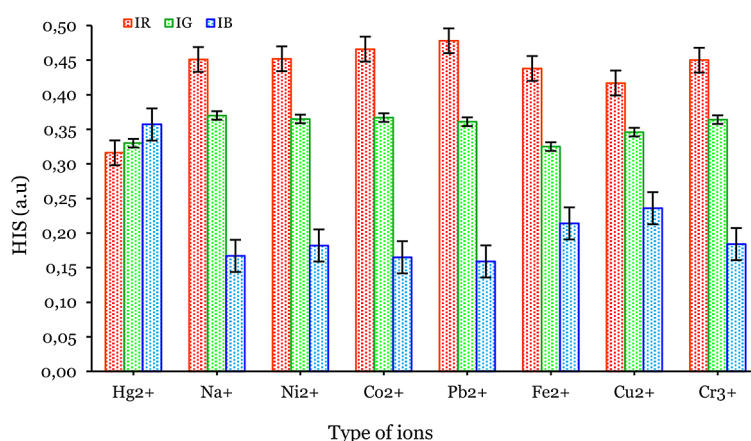


Figure 9. Selectivity profile of the Hg^{2+} measurement using colorimetric sensor TCS3200 based on the I_R (red), I_G (green), and I_B (blue). The concentration of the Hg^{2+} is 200 ppb and added the interferences ions solutions for red, green, and blue bar is 50, 100, 200 ppb, respectively

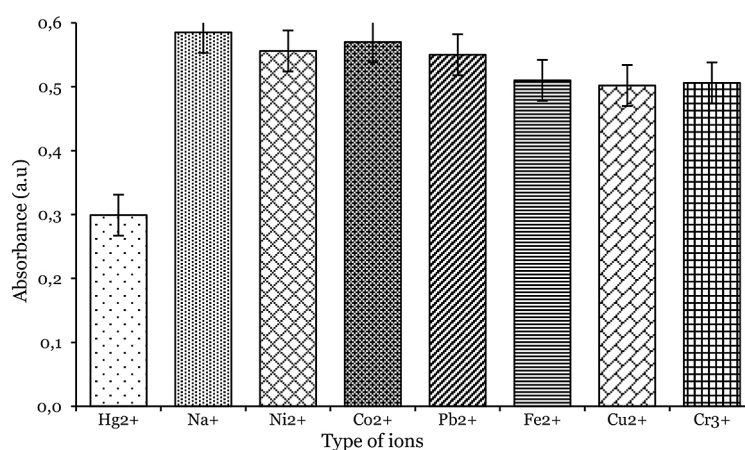


Figure 10. Selectivity profile of the Hg^{2+} measurement using UV-Vis spectrophotometer based on the absorbance

Table 4. Values of RGB and HIS obtained from the measurement of Hg^{2+} content in the samples collected from the river in Aceh Selatan Regency

Samples	RGB			HIS			Color
	R	G	B	IR	IG	IB	
A	222.20 ± 1.483	186.80 ± 0.447	74.00 ± 1.000	0.46 ± 0.001	0.39 ± 0.002	0.15 ± 0.001	
B	224.00 ± 2.915	187.20 ± 0.447	72.80 ± 0.447	0.46 ± 0.003	0.39 ± 0.002	0.15 ± 0.002	
C	226.60 ± 1.140	187.40 ± 0.548	72.20 ± 0.837	0.47 ± 0.002	0.39 ± 0.001	0.15 ± 0.002	
D	227.80 ± 0.447	188.00 ± 1.000	71.00 ± 0.707	0.47 ± 0.002	0.39 ± 0.001	0.15 ± 0.001	
E	217.00 ± 0.707	179.00 ± 0.707	65.00 ± 0.707	0.47 ± 0.001	0.39 ± 0.001	0.14 ± 0.001	

Notes: RGB – red green blue; HIS – hue intensity saturation; R – red; G – green; B – blue; IR – IG – IB – index of color: red, green, blue, respectively; mean ± standard deviation.

IB value. The concentrations of Hg^{2+} in the river water samples as determined by using the colorimetric sensor TCS3200 with AgNP/PVP have been presented in Figure 11. The concentration ranged from $76.8 \pm 2.28 \mu\text{g/L}$ (Sample A) to $52.0 \pm 2.28 \mu\text{g/L}$ (Sample E). Sample A was collected at 3.154594°N and 97.374343°E , whilst Sample B – 3.154876°N and 97.374945°E . The mercury (Hg^{2+}) levels measured in the river in Aceh Selatan Regency, Aceh, Indonesia exceed the threshold set by the World Health Organization (WHO) (WHO, 2008).

Comparisons of the Hg^{2+} concentrations obtained through the colorimetric sensor TCS3200 versus UV-vis spectrophotometer

The comparisons for Hg^{2+} concentrations obtained by using the colorimetric sensor TCS3200 versus UV-vis spectrophotometer presented in Table 5. The experimental t values for Sample A, B, C, D, and E were 0.125, 0.483, 0.181, 0.515, and 0.633, respectively. Experimental t

values obtained herein were less than the theoretical t value which happened to be 2.31 at 95% confidence interval. This suggests that the Hg^{2+} concentrations obtained from colorimetric sensor TCS3200 and UV-vis spectrophotometer were not significantly different. This finding highlights the reliability and accuracy of the TCS3200 sensor in detecting Hg^{2+} in river water samples, comparable to the standard UV-vis spectrophotometry method. The absence of significant differences suggests that the TCS3200 sensor can serve as a cost-effective and portable alternative for on-site mercury detection, addressing the limitations of conventional laboratory-based spectrophotometric methods, such as higher costs, non-portability, and complex operational protocols. Future work could focus on scaling up the production of the sensor components, automating sample preparation steps, and integrating the sensor into existing industrial monitoring systems. This would enhance its practicality and reliability for large-scale environmental or industrial applications.

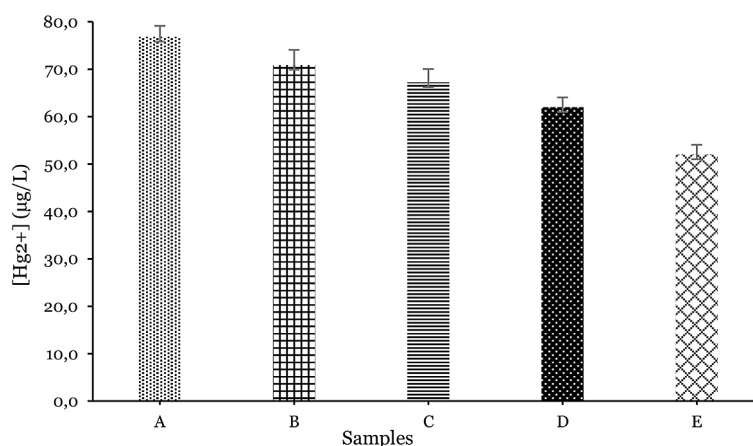


Figure 11. Concentrations of Hg^{2+} in river water samples determination using colorimetric sensor TCS3200 with AgNPs/PVP indicators

Table 5. Comparison of the colorimetric sensor TCS3200 versus UV-vis spectrophotometer in the determination of Hg²⁺ concentrations in river water samples

Samples	Concentration (µg/L)		t _{experimental}	t _{theoretical} (df: 8, α: 0.005)
	TCS3200	UV-Vis		
A	76.80 ± 2.332 ^a	77.11 ± 1.460 ^a	0.125	2.31
B	70.87 ± 3.204 ^a	71.67 ± 1.452 ^a	0.483	
C	67.20 ± 2.828 ^a	67.41 ± 1.464 ^a	0.181	
D	62.00 ± 2.040 ^a	62.53 ± 2.451 ^a	0.515	
E	52.00 ± 2.040 ^a	52.56 ± 2.459 ^a	0.633	

Notes: The same notation indicates that there is no significant difference between the measurement of Hg²⁺ using colorimetric sensor TCS3200 and the UV-Vis spectrophotometer; data presented as mean ± standard deviation.

CONCLUSIONS

The newly developed Hg(II) quantification method using an AgNPs/PVP-stabilized TCS3200 colorimetric sensor demonstrated strong analytical performance, characterized by high accuracy, precision, sensitivity, selectivity, and specificity due to the localized surface plasmon resonance (LSPR) effect. Statistical comparison with UV-Vis spectrophotometry confirmed its reliability, showing no significant differences in measurements. The system, portable and cost-effective, successfully detected Hg(II) in river water samples from Aceh Selatan Regency, with concentrations ranging from 52.0 ± 2.28 to 76.8 ± 2.28 µg/L, proving its practical value for environmental monitoring.

Despite its promise, the method's limitations include dependence on stable lighting conditions and potential interference from competing ions in complex matrices, requiring careful calibration. Future studies should optimize factors such as AgNPs/PVP solution volume and reaction time to enhance sensitivity and stability. Moreover, a thorough characterization of sample matrices, including pH, ionic strength, and dominant ions, is recommended to better understand environmental impacts on sensor performance. These improvements will ensure greater robustness and adaptability for broader applications in diverse environmental contexts.

REFERENCES

- Abdel-Lateef, M. A., Almahri, A., Alzahrani, E., Pashameah, R. A., Abu-Hassan, A. A., & El Hamd, M. A. (2022). Sustainable PVP-Capped Silver nanoparticles as a free-standing nanozyme sensor for visual and spectrophotometric detection of Hg²⁺ in water samples: A green analytical method. *Chemosensors*, 10(9), 358. <https://doi.org/10.3390/chemosensors10090358>
- Ahmad, K., Iqhrammullah, M., Rizki, D. R., Aulia, A., Mairizal, A. Q., Purnama, A., Qanita, I., Abdulmajid, S. N., & Puspita, K. (2022). Heavy metal contamination in aquatic and terrestrial animals resulted from anthropogenic activities in Indonesia: A review. *Asian Journal of Water, Environment and Pollution*, 19, 1–8. <https://doi.org/10.3233/AJW220049>
- Amatongchai, M., Sitanurak, J., Sroysee, W., Sodanat, S., Chairam, S., Jarujamrus, P., Nacapricha, D., & Lieberzeit, P. A. (2019). Highly sensitive and selective electrochemical paper-based device using a graphite screen-printed electrode modified with molecularly imprinted polymers coated Fe₃O₄@Au@SiO₂ for serotonin determination. *Analytica Chimica Acta*, 1077, 255–265. <https://doi.org/10.1016/j.aca.2019.05.047>
- Amirjani, A., & Fatmehsari, D. H. (2018). Colorimetric detection of ammonia using smartphones based on localized surface plasmon resonance of silver nanoparticles. *Talanta*, 176, 242–246. <https://doi.org/10.1016/j.talanta.2017.08.022>
- Balasurya, S., Syed, A., Thomas, A. M., Marraiki, N., Elgorban, A. M., Raju, L. L., Das, A., & Khan, S. S. (2020). Rapid colorimetric detection of mercury using silver nanoparticles in the presence of methionine. *Spectrochimica Acta Part A: Molecular and Biomolecular Spectroscopy*, 228, 117712. <https://doi.org/https://doi.org/10.1016/j.saa.2019.117712>
- Brambilla, M., Romano, E., Buccheri, M., Cutini, M., Toscano, P., Cacini, S., Massa, D., Ferri, S., Monarca, D., Fedrizzi, M., Burchi, G., & Bisaglia, C. (2021). Application of a low-cost RGB sensor to detect basil (*Ocimum basilicum* L.) nutritional status at pilot scale level. *Precision Agriculture*, 22(3), 734–753. <https://doi.org/10.1007/s11119-020-09752-0>
- Chen, Z., Chang, J. W., Balasanthiran, C., Milner, S. T., & Rioux, R. M. (2019). Anisotropic growth of silver nanoparticles is kinetically controlled by polyvinylpyrrolidone binding. *Journal of the*

- American Chemical Society*, 141(10), 4328–4337. <https://doi.org/10.1021/jacs.8b11295>
8. Diamai, S., & Negi, D. P. S. N. (2020). Colorimetric detection of Pb²⁺ ions using PVP-capped silver nanoparticles. *The NEHU Journal*, 18(1), 33–41. <https://api.semanticscholar.org/CorpusID:222119812%7D>
 9. Environmental Protection Agency. (2024). *National Primary Drinking Water Regulations*. <https://www.epa.gov/ground-water-and-drinking-water/national-primary-drinking-water-regulations>
 10. Fernández-Ramos, M. D., Moreno-Puche, F., Escobedo, P., García-López, P. A., Capitán-Vallvey, L. F., & Martínez-Olmos, A. (2020). Optical portable instrument for the determination of CO₂ in indoor environments. *Talanta*, 208, 120387. <https://doi.org/10.1016/j.talanta.2019.120387>
 11. Fiorati, A., Bellingeri, A., Punta, C., Corsi, I., & Venditti, I. (2020). Silver nanoparticles for water pollution monitoring and treatments: Ecosafety challenge and cellulose-based hybrids solution. *Polymers*, 12(8), 1635. <https://doi.org/10.3390/polym12081635>
 12. Fitri, Z., Adlim, M., Syukri Surbakti, M., Fairuz Omar, A., Ananda Sijabat, F., & Syahreza, S. (2019). Mercury (II) Ions Assessment as a Toxic Waste Hazard in Solution Based on Imagery Data for a Part of Environmental Disaster Management. *IOP Conference Series: Earth and Environmental Science*, 273(1), 012052. <https://doi.org/10.1088/1755-1315/273/1/012052>
 13. Gusrizal, G., Alimuddin, A. H., Sapar, A., Ridwan, R. N., & Santosa, S. J. (2019). Colorimetric detection of Hg(II) ion using silver nanoparticles capped with 3-Hydroxybenzoic acid. *Molekul*, 14(1), 18. <https://doi.org/10.20884/1.jm.2019.14.1.460>
 14. Hasan, A., Nanakali, N. M. Q., Salihi, A., Rasti, B., Sharifi, M., Attar, F., Derakhshankhah, H., Mustafa, I. A., Abdulqadir, S. Z., & Falahati, M. (2020). Nanozyme-based sensing platforms for detection of toxic mercury ions: An alternative approach to conventional methods. *Talanta*, 215, 120939. <https://doi.org/https://doi.org/10.1016/j.talanta.2020.120939>
 15. Huang, J., Mo, X., Fu, H., Sun, Y., Gao, Q., Chen, X., Zou, J., Yuan, Y., Nie, J., & Zhang, Y. (2021). Tyndall-effect-enhanced supersensitive naked-eye determination of mercury (II) ions with silver nanoparticles. *Sensors and Actuators B: Chemical*, 344, 130218. <https://doi.org/https://doi.org/10.1016/j.snb.2021.130218>
 16. Jabbar, A., Abbas, A., Assad, N., Naeem-ul-Hassan, M., Alhazmi, H. A., Najmi, A., Zoghebi, K., Al Bratty, M., Hanbashi, A., & Amin, H. M. A. (2023). A highly selective Hg²⁺ colorimetric sensor and antimicrobial agent based on green synthesized silver nanoparticles using Equisetum diffusum extract. *RSC Advances*, 13(41), 28666–28675. <https://doi.org/10.1039/D3RA05070J>
 17. Janani, B., Syed, A., Thomas, A. M., Bahkali, A. H., Elgorban, A. M., Raju, L. L., & Khan, S. S. (2020). UV–vis spectroscopic method for the sensitive and selective detection of mercury by silver nanoparticles in presence of alanine. *Optik*, 204, 164160. <https://doi.org/10.1016/j.ijleo.2019.164160>
 18. Kemala, P., Idroes, R., Khairan, K., Ramli, M., Jalil, Z., Idroes, G. M., Tallei, T. E., Helwani, Z., Safitri, E., Iqhrammullah, M., & Nasution, R. (2022). Green synthesis and antimicrobial activities of silver nanoparticles using calotropis gigantea from ie seu-um geothermal area, Aceh Province, Indonesia. *Molecules*, 27(16), 5310. <https://doi.org/10.3390/molecules27165310>
 19. Lin, Y., Zhou, Q., Tang, D., Niessner, R., Yang, H., & Knopp, D. (2016). Silver nanolabels-assisted ion-exchange reaction with CdTe quantum dots mediated exciton trapping for signal-on photoelectrochemical immunoassay of mycotoxins. *Analytical Chemistry*, 88(15), 7858–7866. <https://doi.org/10.1021/acs.analchem.6b02124>
 20. Meenakshi, S., Devi, S., Pandian, K., Chitra, K., & Tharmaraj, P. (2019). Aniline-mediated synthesis of carboxymethyl cellulose protected silver nanoparticles modified electrode for the differential pulse anodic stripping voltammetry detection of mercury at trace level. *Ionics*, 25(7), 3431–3441. <https://doi.org/10.1007/s11581-019-02858-0>
 21. Monisha, Shrivastava, K., Kant, T., Patel, S., Devi, R., Dahariya, N. S., Pervez, S., Deb, M. K., Rai, M. K., & Rai, J. (2021). Inkjet-printed paper-based colorimetric sensor coupled with smartphone for determination of mercury (Hg²⁺). *Journal of Hazardous Materials*, 414, 125440. <https://doi.org/https://doi.org/10.1016/j.jhazmat.2021.125440>
 22. Nisah, K., Muslem, M., Ashari, T., Afkar, M., & Iqhrammullah, M. (2022). Distribution of Mercury in Soil, Water, and Vegetable Fern in a Former Gold Mining Area – Evidence from Nagan Raya Regency, Aceh Province, Indonesia. *Journal of Ecological Engineering*, 23(8), 30–39. <https://doi.org/10.12911/22998993/150684>
 23. Nisah, K., Rahmi, R., Ramli, M., Idroes, R., Alva, S., Iqhrammullah, M., & Safitri, E. (2022). Optimization of castor oil-based ion selective electrode (ISE) with Active Agent 1,10-Phenanthroline for Aqueous Pb²⁺ Analysis. *Membranes*, 12(10), 987. <https://doi.org/10.3390/membranes12100987>
 24. Nisah, K., Rahmi, Ramli, M., Iqhrammullah, M., Mitaphonna, R., Hartadi, B. S., Abdulmadjid, S. N., Md Sani, N. D., Idroes, R., & Safitri, E. (2022). Controlling the diffusion of micro-volume Pb solution on hydrophobic polyurethane membrane for

- quantitative analysis using laser-induced breakdown spectroscopy (LIBS). *Arabian Journal of Chemistry*, 15(6), 103812. <https://doi.org/10.1016/j.arabjc.2022.103812>
25. Pomal, N. C., Bhatt, K. D., Modi, K. M., Desai, A. L., Patel, N. P., Kongor, A., & Kolivoška, V. (2021). Functionalized silver nanoparticles as colorimetric and fluorimetric sensor for environmentally toxic mercury ions: An overview. *Journal of Fluorescence*, 31(3), 635–649. <https://doi.org/10.1007/s10895-021-02699-z>
 26. Puchum, S., Meelapsom, R., Muniandy, S. S., Lee, H. L., Pencharee, S., Amatatongchai, M., Suttisintong, K., & Jarujamrus, P. (2019). Use of unmodified silver nanoparticles (AgNPs) as colorimetric Hg(II) sensor: A new approach to sensitive and high sample throughput determination of Hg(II) under high influence of ionic suppression. *International Journal of Environmental Analytical Chemistry*, 99(2), 139–156. <https://doi.org/10.1080/03067319.2019.1580703>
 27. Rahmi, Julinawati, Nina, M., Fathana, H., & Iqhrammullah, M. (2022). Preparation and characterization of new magnetic chitosan-glycine-PEGDE (Fe₃O₄/Ch-G-P) beads for aqueous Cd(II) removal. *Journal of Water Process Engineering*, 45, 102493. <https://doi.org/10.1016/j.jwpe.2021.102493>
 28. Rajar, K., Alveroglu, E., Caglar, M., & Caglar, Y. (2021). Highly selective colorimetric onsite sensor for Co²⁺ ion detection by povidone capped silver nanoparticles. *Materials Chemistry and Physics*, 273, 125082. <https://doi.org/10.1016/j.matchemphys.2021.125082>
 29. Ren, H., Zhang, Q., Meng, Z., Ling, R., Qin, W., & Wu, Z. (2021). Online monitoring strategies for colorimetric detection of cadmium ions and pH Based on gold nanomaterials with a low-cost color sensor. *ACS Sustainable Chemistry & Engineering*, 9(17), 5924–5932. <https://doi.org/10.1021/acssuschemeng.1c00238>
 30. Sakly, N., Marzouk, W., Ouada, H. Ben, & Majdoub, H. (2017). Enhancing performances of colorimetric response of carboxymethylcellulose-stabilized silver nanoparticles: A fully eco-friendly assay for Hg²⁺ detection. *Sensors and Actuators B: Chemical*, 253, 918–927. <https://doi.org/10.1016/j.snb.2017.07.035>
 31. Sánchez-Alarcón, J., Milić, M., Bustamante-Montes, L. P., Isaac-Olivé, K., Valencia-Quintana, R., & Ramírez-Durán, N. (2021). Genotoxicity of mercury and its derivatives demonstrated in vitro and in vivo in human populations studies. Systematic review. *Toxics*, 9(12), 326. <https://doi.org/10.3390/toxics9120326>
 32. Sandra, Damayanti, R., & Inayah, Z. (2020). Nitrogen Fertilizer Prediction of Maize Plant with TCS3200 Sensor Based on Digital Image Processing. *IOP Conference Series: Earth and Environmental Science*, 515(1), 012014. <https://doi.org/10.1088/1755-1315/515/1/012014>
 33. Schiesaro, I., Burratti, L., Meneghini, C., Fratoddi, I., Proposito, P., Lim, J., Scheu, C., Venditti, I., Iucci, G., & Battocchio, C. (2020). Hydrophilic Silver Nanoparticles for Hg(II) Detection in Water: Direct Evidence for Mercury–Silver Interaction. *The Journal of Physical Chemistry C*, 124(47), 25975–25983. <https://doi.org/10.1021/acs.jpcc.0c06951>
 34. Shrivastava, K., Sahu, B., Deb, M. K., Thakur, S. S., Sahu, S., Kurrey, R., Kant, T., Patle, T. K., & Jangde, R. (2019). Colorimetric and paper-based detection of lead using PVA capped silver nanoparticles: Experimental and theoretical approach. *Microchemical Journal*, 150, 104156. <https://doi.org/10.1016/j.microc.2019.104156>
 35. Shukla, G. M., Punjabi, N., Kundu, T., & Mukherji, S. (2019). Optimization of plasmonic u-shaped optical fiber sensor for mercury ions detection using glucose capped silver nanoparticles. *IEEE Sensors Journal*, 19(9), 3224–3231. <https://doi.org/10.1109/JSEN.2019.2893270>
 36. Singh, H., Singh, G., Mahajan, D. K., Kaur, N., & Singh, N. (2020). A low-cost device for rapid ‘color to concentration’ quantification of cyanide in real samples using paper-based sensing chip. *Sensors and Actuators B: Chemical*, 322, 128622. <https://doi.org/10.1016/j.snb.2020.128622>
 37. Suhud, K., Sukoma, S., Saleha, S., & Surbakti, M. S. (2024). Development of TCS3200 color sensor based on arduino uno and its application in determining borax levels in food. *Indonesian Journal of Fundamental and Applied Chemistry*, 9(2), 74–81. <https://doi.org/10.24845/ijfac.v9.i2.74>
 38. Surbakti, M. S., Farhan, M., Zakaria, Z., Isa, M., Sufridi, E., Alva, S., Yusibani, E., Heliawati, L., Iqhrammullah, M., & Suhud, K. (2022). Development of arduino uno-based TCS3200 color sensor and its application on the determination of Rhodamine B level in Syrup. *Indonesian Journal of Chemistry*, 22(1), 630. <https://doi.org/10.22146/ijc.69214>
 39. Galatage, S.T., Hebalkar, A.S., V. Dhobale, S., Mali, O.R., Kumbhar, P. S., Nikade, S.V., & Killedar, S.G. (2021). Silver nanoparticles: Properties, synthesis, characterization, applications and future trends. In *Silver Micro-Nanoparticles - Properties, Synthesis, Characterization, and Applications*. IntechOpen. <https://doi.org/10.5772/intechopen.99173>
 40. Tanvir, F., Yaqub, A., Tanvir, S., An, R., & Anderson, W. A. (2019). Colorimetric detection of mercury ions in water with capped silver nanoprisms. *Materials*, 12(9), 1533. <https://doi.org/10.3390/ma12091533>
 41. Wang, H., Tang, J., Wan, X., Wang, X., Zeng, Y.,

- Liu, X., & Tang, D. (2024). Mechanism exploration of the photoelectrochemical immunoassay for the integration of radical generation with self-quenching. *Analytical Chemistry*, 96(38), 15503–15510. <https://doi.org/10.1021/acs.analchem.4c04050>
42. Wang, Y., Zeng, R., Tian, S., Chen, S., Bi, Z., Tang, D., & Knopp, D. (2024). Bimetallic single-atom nanozyme-based electrochemical-photothermal dual-function portable immunoassay with smartphone imaging. *Analytical Chemistry*, 96(33), 13663–13671. <https://doi.org/10.1021/acs.analchem.4c02606>
43. WHO. (2008). *WHO Guidelines for Drinking-Water Quality*. 35(5), 307–312. <https://doi.org/10.1248/jhs1956.35.307>
44. Xu, M., Gao, Z., Wei, Q., Chen, G., & Tang, D. (2016). Label-free hairpin DNA-scaffolded silver nanoclusters for fluorescent detection of Hg²⁺ using exonuclease III-assisted target recycling amplification. *Biosensors and Bioelectronics*, 79, 411–415. <https://doi.org/10.1016/j.bios.2015.12.081>
45. Zhou, Q., Lin, Y., Xu, M., Gao, Z., Yang, H., & Tang, D. (2016). Facile synthesis of enhanced fluorescent gold–silver bimetallic nanocluster and its application for highly sensitive detection of inorganic pyrophosphatase activity. *Analytical Chemistry*, 88(17), 8886–8892. <https://doi.org/10.1021/acs.analchem.6b02543>
46. Zhou, Y., Saidi, W.A., & Fichthorn, K.A. (2014). A Force field for describing the polyvinylpyrrolidone-mediated solution-phase synthesis of shape-selective Ag nanoparticles. *The Journal of Physical Chemistry C*, 118(6), 3366–3374. <https://doi.org/10.1021/jp412098n>
47. Zhu, L., Yin, Z., Lv, Z., Li, M., & Tang, D. (2021). Ultrasensitive photoelectrochemical immunoassay for prostate-specific antigen based on silver nanoparticle-triggered ion-exchange reaction with ZnO/CdS nanorods. *The Analyst*, 146(14), 4487–4494. <https://doi.org/10.1039/D1AN00822F>